The Orion Complex Revisited
ASP Conference Series, Vol. 999, 1999
M. J. McCaughrean, ed.

High-Resolution Submillimetre/Millimetre Interferometry of the Orion-KL Region

Katharina Schreyer, Thomas Henning

Astrophysikalisches Institut und Universitäts-Sternwarte,
Schillergäßchen 2-3, D-07745 Jena, Germany
martin & henning@astro.uni-jena.de

Helmut Wiesemeyer

Institut de Radio Astronomie Millimétrique,
300, Rue de la Piscine, F-38406 St.-Martin-d'Héres Cedex, France
wiesemeyer@iram.fr

Abstract. We review the structure of the Orion-KL region, an active site of high-mass star formation embedded in OMC-1, as derived from high-resolution submillimetre and millimetre observations. We discuss the different components of the OMC-1 cloud core and their relation to the energy sources in this region. We also present the results of line observations in transitions of the CH_3CN and $C^{34}S$ molecules carried out with the Plateau de Bure interferometer.

1. Introduction

The region of the Kleinmann-Low infrared nebula (henceforth Orion-KL; Kleinmann & Low 1967) in the Orion molecular cloud 1 (OMC-1) behind the Orion Nebula is a "holy grail" in the study of star formation since it is the nearest location where high-mass stars are presently being formed (Genzel & Stutzki 1989). Nevertheless, despite its relatively small distance of ~ 500 pc, one needs observations with high angular resolution to gain an insight into the massive stellar birth process comparable to that which we have for the three times closer regions of low-mass star formation such as Taurus-Auriga and Chamaeleon. This is even more the case when we consider the relatively complicated structure of the inner cloud core of OMC-1. High angular resolution millimetre interferometer and infrared studies of this region started some ten years ago, and it the goal of this chapter to give a general overview of the results obtained by these observations. Furthermore, we will discuss data from the Plateau de Bure interferometer in the CH_3CN J=5–4 and $C^{34}S$ J=2–1 transitions which very nicely demonstrate the potential of molecular line interferometry.

2. Structure of Orion-KL: High-Resolution Data

2.1. The sources of luminosity

High angular resolution infrared images of Orion-KL have been made in the wavelength range 2–30 μm by Rieke, Low, & Kleinmann (1973), Downes *et al.* (1981), Grasdalen,

Gehrz, & Hackwell (1981), Lonsdale *et al.* 1982; Lee *et al.* (1983), Wynn-Williams *et al.* (1984), Gezari (1992), and Gezari, Backman, & Werner (1998) (see also the chapter by Deutsch *et al.*), and altogether more than ten individual infrared objects were found to be located in an area of 20×20 arcsec. Several lines of evidence point to the fact that many of these infrared sources are not self-luminous, but that they may only represent reprocessed radiation leaking out through the inhomogeneous cloud material surrounding the main energy source(s) or just light scattered off dense clumps (Downes *et al.* 1981; Minchin *et al.* 1991; Dougados *et al.* 1993). Through mid-infrared mapping (Downes *et al.* 1981; Wynn-Williams *et al.* 1984; Dougados *et al.* 1993) and additional polarization measurements (Werner, Capps, & Dinerstein 1983; Wynn-Williams *et al.* 1984; Minchin *et al.* 1991) of the Orion-KL region, the main energy source of the region turned out to be one or more deeply embedded objects close to or associated with IRc2. This powerful source (or sources) must play a central role for the thermal and dynamical structure of the whole region.

The total observed luminosity from the region is on the order of $10^5\,L_\odot$ (Werner *et al.* 1976; Genzel *et al.* 1982; Drapatz *et al.* 1983; Jaffe *et al.* 1984; Chelli, Perrier, & Léna 1984; Wynn-Williams *et al.* 1984; Thronson *et al.* 1986) and the region is seen to be the source of a high-velocity outflow observed in SiO and H_2 (Beckwith *et al.* 1978; Wright *et al.* 1983; Allen & Burton 1993; Sugai *et al.* 1994). Downes *et al.* (1981) suggested that a single source, IRc2, produces most of the luminosity and drives the outflow, but later high-resolution near-infrared observations by Dougados *et al.* (1993) showed that IRc2 was not a discrete source, but at the subarcsecond level breaks up into four subcondensations named IRc2-A, B, C, and D. Similar high angular resolution observations at infrared, millimetre, and radio wavelengths have shown the region to be considerably more complicated than previously expected.

One particular problem is that many of the near- and mid-infrared sources many not be self-luminous, but rather are clumps of dust illuminated by embedded or nearby sources. One way of ascertaining which are the true sources of luminosity is to search for compact radio continuum sources, as signposts of ultracompact H II regions and thus deeply embedded massive stars: this has been done by several groups for the Orion-KL region (*e.g.*, Garay, Moran, & Reid 1987; Churchwell *et al.* 1987; Felli *et al.* 1993; Menten & Reid 1995; see also the chapter by Felli & Churchwell). The most prominent compact radio sources are B, I, and L[1], and these are presently felt to be the main luminosity sources in the region.

Radio source B is the Becklin-Neugebauer (BN) object, the brightest source in the region at near-infrared wavelengths (Becklin & Neugebauer 1967; Foy *et al.* 1979; Scoville *et al.* 1983). Although the BN object originally attracted significant attention because it was thought to be a massive protostar, more recent interpretations have shifted towards it being a deeply embedded B-type star with a luminosity of $\sim 2500\,L_\odot$ coming from the core source and a total of $\sim 10000\,L_\odot$ when the surrounding diffuse plateau of emission is also included (Gezari *et al.* 1998; Henning 1990).

[1]In general, sources in the Orion-KL region with capital letter identifiers such as B, I, and L are radio continuum sources following the nomenclature of Garay *et al.* (1987) and Churchwell *et al.* (1987), while lowercase identifiers such as g, n, and t refer to near-infrared sources in the region catalogued by Lonsdale *et al.* (1982). As noted by Menten & Reid (1985) however, the letter L was independently assigned to two separate radio sources by Garay (1987) and Gezari (1992): in this chapter, we follow Gezari (1992) in using L to refer to the radio source coincident with the near-infrared source n.

Radio source I is close to IRc2 and invisible at infrared wavelengths. Based on his mid-infrared imaging, Gezari (1992) reported an offset of ~ 0.8 arcsec between source I and the nominal IRc2 position, while Menten & Reid (1995) found an offset of ~ 0.5 arcsec between source I and IRc2-A of Dougados *et al.* (1993). It seems likely that the position of the radio source coincides with the actual location of the embedded object, and that the infrared source IRc2-A is simply scattered light, an interpretation which would be in agreement with the high degree of polarization measured at that position.

Several authors (Baud *et al.* 1980; Wright & Plambeck 1983; Wright *et al.* 1990) reported the detection of a powerful SiO maser at a position close to IRc2 and coincident with a 'shell' of H_2O masers (Moran *et al.* 1977). SiO masers are generally associated with late-type stars, and are only very rarely found in star-forming regions, where their presence is taken as evidence for a high-luminosity source with $> 10^4\,L_\odot$. Based on the SiO maser spectrum, Wright *et al.* (1990, 1995) proposed that the maser emission originates in a rotating and expanding 80–1000 AU diameter ring. Subsequent VLA observations by Menten & Reid (1995) and BIMA observations by Wright *et al.* (1995) resolved the velocity components of the SiO maser emission, and both teams concluded that the distribution could in general be reproduced by the model of a maser ring developed by Barvainis (1984) and Plambeck, Wright, & Carlstrom (1990). More recent very high spatial resolution VLBA studies (Greenhill *et al.* 1998; Doeleman, Lonsdale, & Pelkey 1999) have resulted in a quite different hypothesis, in which the SiO masers are formed in shocks and overdense clumps in a NW-SE bipolar outflow oriented quite close to the line-of-sight. The coincident shell of H_2O masers, seen covering an elongated 2×0.5 arcsec region oriented NE-SW (Gaume *et al.* 1998), then traces either another part of the same flow (Doeleman *et al.* 1999) or a second flow (Greenhill *et al.* 1998).

In the context of the present discussion, the most important point about the SiO and H_20 maser clusters is that both are closely coincident with the position of the radio continuum source I, and thus not with any of the near-infrared components of IRc2 (Menten & Reid 1995; Gaume *et al.* 1998). This finding effectively relegates IRc2 to the status of an 'also ran' source, with the most recent estimate of its luminosity being only $\sim 1000\,L_\odot$ (Gezari *et al.* 1998). Source I, on the other hand, must be a major source of luminosity: although no direct estimate can be made as it is not detected at near- or mid-infrared wavelengths, the central star must have $>$ a few thousand $L_\odot$ in order to power an H II region, and the SiO masers point to something even more luminous.

Finally, the role played by radio continuum source L plays remains open. It lies ~ 3 arcsec southwest of IRc2-A (Genzel *et al.* 1982; Hermsen, Wilson, & Bieging 1988; Migenes *et al.* 1989; Gezari 1992; Menten & Reid 1995; Gezari *et al.* 1998), and has a peculiar double-lobed structure (Menten & Reid 1995). It has a bright near-infrared counterpart, source n (Lonsdale *et al.* 1982; Wynn-Williams *et al.* 1984; Dougados *et al.* 1993), although it is nothing like as red as the IRc2 sub-components, and Lonsdale *et al.* (1982) classified it simply s a reddened star. Nevertheless, the double-lobed and variable radio continuum emission from source L (Menten & Reid 1995) marks it out as another self-luminous energetic source and indeed, it is located right at the centre of the dominant low-velocity H_2O maser outflow (Genzel *et al.* 1981), and thus is a plausible candidate for the driving source of the broader outflows seen in the region.

2.2. Molecular clumps and cores

The molecular cloud core of OMC-1 has been the subject of many radio continuum and line studies. A list of high-resolution studies in different line transitions using several

Authors	Array	Maps	Beam size
Blake *et al.* (1996)	OVRO	218 GHz cont., SiO ν5–4, HC_3N, $HCOOCH_3$, C_2H_5CN, HNCO, HDO	$2'' \times 1.5''$, $1.5'' \times 1''$
Chandler & DePree (1995)	VLA	SiO ν1–0, $v = 0$	$2.13'' \times 1.83''$
Chernin & Wright (1996)	BIMA	CO ν1–0	$3.2'' \times 2.6''$
Doeleman *et al.* (1999)	VLBA	SiO ν1–0, $v = 1$ maser	$0.39'' \times 0.175''$
Gaume *et al.* (1998)	VLA	H_2O ν6 $_{16}$–5_{23} maser	$0.1'' \times 0.09''$
Genzel *et al.* (1982)	VLA	NH_3 (3,2), (4,4), (4,2)	$2.7''$
Genzel *et al.* (1981)	VLBI	22 GHz H_2O maser	few milliarcsec
Hermsen *et al.* (1988)	VLA	NH_3 (4,3)	$1.88'' \times 1.86''$
Mangum *et al.* (1993)	VLA	H_2CO ν1 $_{10}$–1_{11}	$5.9'' \times 4.4''$
	BIMA	H_2CO ν5 $_{14}$–5_{15}	$7.9'' \times 7.4''$
Masson *et al.* (1985)	MWI	112.6, 112.9 GHz cont.	$5.8'' \times 8.7''$, $6.5'' \times 12.4''$
Masson *et al.* (1987)	MWI	CO, ^{13}CO ν1–0	$5.8'' \times 8.7''$, $6.5'' \times 12.4''$
Masson & Mundy (1988)	OVRO	HC_3N ν12–11	$4''$
Menten & Reid (1995)	VLA	SiO ν1–0, $v = 1$, maser, 43.1, 8.4 GHz cont.	$0.25''$, $0.22''$
Migenes *et al.* (1989)	VLA	NH_3 (3,2)	$1.24'' \times 1.2''$
Minh *et al.* (1993)	NMA	88 GHz cont., CH_3OH ν15 $_3$–14_4 A^-, $(CH_3)_2O$ ν15 $_{2,13}$–$15_{1,14}$, $HCOOCH_3$ ν7 $_{1,6}$–$6_{1,5}$ E,A	$5.2'' \times 4.2''$
Mundy *et al.* (1986)	OVRO	95 GHz cont., CS ν2–1	$7.5''$
Murata & Hasegawa (1990)	NMA	NH_3 (1,1), (2,2)	$6'' \times 10''$
Murata *et al.* (1991)	NMA	95 GHz cont., CS ν1–0, 2–1	$6'' \times 8''$, $2'' \times 3''$
Pauls *et al.* (1983)	VLA	NH_3 (3,3)	$2.2'' \times 1.6''$
Plambeck *et al.* (1982)	HC	86 GHz cont., SO ν2 $_2$–1_1	$6'' \times 6''$
Plambeck *et al.* (1995)	BIMA	86 GHz cont.	$1'' \times 0.38''$, $1.67'' \times 0.76''$
Plambeck *et al.* (1990)	HC	SiO ν2–1, $v = 1$, maser	$2.6'' \times 1.5''$
Plambeck & Wright (1987)	HC	HDO ν1 $_{10}$–1_{11}	$3.5'' \times 3.3''$
Rao *et al.* (1998)	BIMA	1.3, 3.3 mm continuum polarization	$4.4'' \times 2.4''$, $6.8'' \times 2.8''$
Schilke *et al.* (1992)	PdB	86 GHz cont., $HC^{15}N$ ν1–0	$5.3'' \times 4.5''$
Wilner *et al.* (1994)	HC	CH_3CN ν5–4	$6.5'' \times 5.5''$, $4.1'' \times 3.5''$
Wilson *et al.* (1996)	VLA	NH_3 (10,9)	
Wright *et al.* (1996)	BIMA	86 GHz cont., H_2CO, DCN, HDO, CH_3CH_2CN, HC_3N, SO_2, SO, OCS, ^{29}SiO, SiO, $H^{13}CN$, HCN, HCO^+, CH_3CN, CH_3OH, CO, NH_2D	$1.7'' \times 0.8''$–$7.3'' \times 5.1''$
Wright *et al.* (1995)	BIMA	SiO ν2–1, $v = 0$,1	$1.7'' \times 0.7''$
Wright *et al.* (1990)	HC	SiO ν2–1, v= 1, maser	$2.4'' \times 1.5''$
Wright & Vogel (1985)	HC	86–89 GHz cont.	$4.4'' \times 2.4''$
Wright *et al.* (1992)	HC	82–95 GHz cont.	$6.9'' \times 5.1''$
Wright *et al.* (1983)	HC	SiO ν2–1, v= 0	$2'' \times 2''$

Key: PdB: Plateau de Bure interferometer; BIMA: Berkeley-Illinois-Maryland-Association Array; MWI: Caltech Millimeter-Wave Interferometer; HC: Hat Creek interferometer; NMA: Nobeyama Millimetre Array; OVRO: Owens Valley Millimeter-Wave Interferometer; VLA: Very Large Array; VLBI: Very Long Baseline Interferometry; VLBA: Very Long Baseline Array

Table 1. High-resolution submm/mm interferometer maps of Orion-KL.

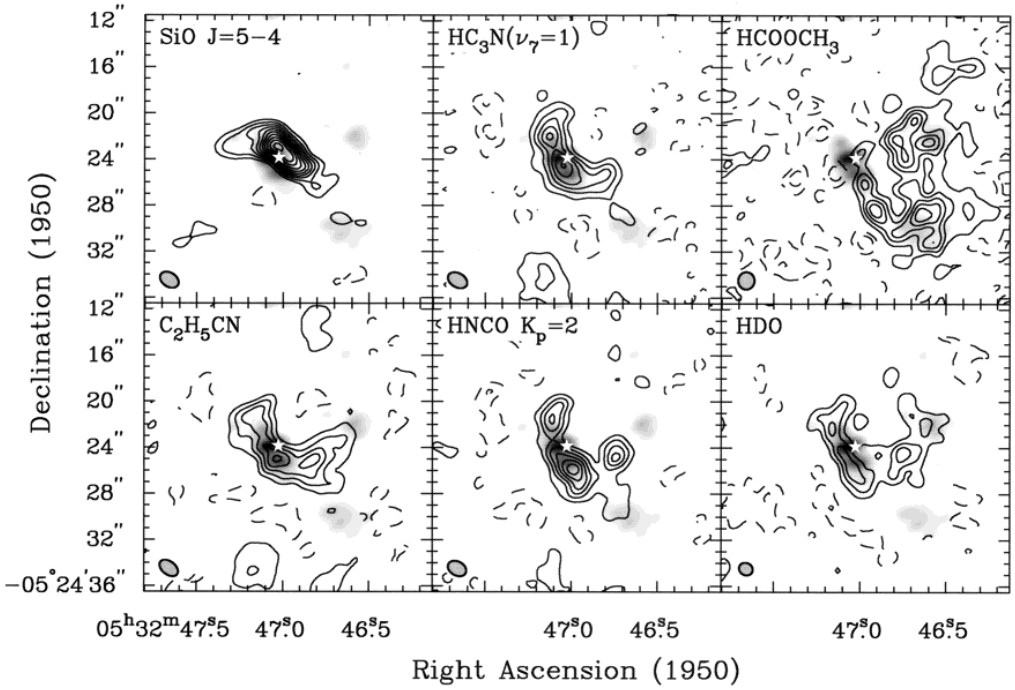

Figure 1. The Orion-KL region seen in different molecular transitions and in continuum at 218 GHz. In each panel, the grayscale presents the uniform-weighted dust continuum emission at 1.5×1.0 arcsec resolution. The contours depict the uniform-weighted maps obtained for selected molecules, noted in the upper left hand corner of each panel. Contour levels for the $HCOOCH_3$ J=20_{417} –19_{416} A transition are spaced by 0.6 Jy beam^{-1} (6 K); for SiO J=5–4 at 0.5 Jy beam^{-1} (8 K); for HDO J=2_{11}–2_{12} and HNCO J=10_{29}–9_{28} at 0.4 Jy beam^{-1} (4 and 7 K); and for HC_3N (v_7=1) J=24–23 ($1f$) and C_2H_5CN J=24_{222} –23_{221} at 0.3 Jy beam^{-1} (5 K); contouring begins at the step level in each case. The white star marks the position of radio source I and the SiO (v=1) maser ring. After Blake *et al.* (1996).

interferometers over the past decade has been compiled in Table 1. An important result of these studies that they show the cloud core of OMC-1 to consist of a number of clumps, each smaller than 2 arcsec, and referring to the results of Wright, Plambeck, & Wilner (1996) and Blake *et al.* (1996), the densest and 'hottest' region (the so-called hot core) appears as a chain of dense clumps, especially in nitrogen-rich components and in the continuum. A selection of the millimetre maps of Orion-KL in different molecular transitions and the dust continuum are shown in Figure 1.

Most of the line studies show that the radio source I is located at the western periphery of the hot core, whereas the infrared source n appears to be centred in the molecular cloud core. Only the SiO measurements by Chandler & DePree (1995) and Wright *et al.* (1996) imply a small elongated structure roughly centred at source I, with a position angle of 50–65°. This small-scale structure is also present in the continuum observations of Plambeck *et al.* (1995). Blake *et al.* (1996) proposed that source I lies behind the dense clumps of the hot core and interacts with them via energetic radiation and a wind from

outside. We should stress that Plambeck *et al.* (1995) found no evidence for protostellar condensations within the core itself in an analysis of their high-resolution continuum measurements.

Following a number of earlier molecular line studies, the inner cloud region of Orion-KL is generally separated in different molecular gas components. For the convenience of the reader, we summarize these components in Table 2, although we should stress that the general appearance of Orion-KL depends on the molecular transition observed and the spatial resolution of the measurements (see, *e.g.*, Figure 1). In fact, many of the structures split up in individual clumps when observed with higher resolution, and to clarify whether or not such clumps are real density enhancements or just temperature peaks always requires a detailed radiative transfer and abundance analysis.

2.3. Molecular outflows

The nature of the different molecular outflow systems in Orion-KL was extensively discussed in the review by Genzel & Stutzki (1989), and here we will only summarize the main properties of the outflows and add the results of a few more recent studies. Broadly, the dynamically-active gas can be separated into the 'low-velocity' (18 km s^{-1} or "expanding doughnut") flow, the 'high-velocity' flow ($\Delta v \leq$ 250 km s $^{-1}$), and the 'high-velocity shock-excited gas' seen in high-velocity H_2O masers and infrared and submillimetre cooling lines.

The low-velocity flow is mainly seen in observations using molecules with higher dipole moments, *e.g.*, SiO (Wright *et al.* 1983) and SO (Plambeck *et al.* 1982), and it can also be identified by the low-velocity H_2O masers (Genzel *et al.* 1981). This flow is orientated in a northeast-southwest direction and forms a kind of expanding gas shell or torus (the 'expanding doughnut') around source I. The line emission covers a full velocity range of $\Delta v_{\rm full} \approx 35\,{\rm km\,s^{-1}}$. Many facts support a model of a spherically-symmetric outflow with the initially freely-streaming gas plunging into the dense ridge gas.

The high-velocity outflow is located approximately perpendicular to the expanding gas shell in the southeast-northwest direction. Studies in CO by Erickson *et al.* (1982), Masson *et al.* (1987), Schulz *et al.* (1995), and Chernin & Wright (1996), and in HCO^+ by Vogel *et al.* (1984), as well as in H_2 by Beckwith *et al.* (1978), Scoville *et al.* (1982), Allen & Burton (1993), Sugai *et al.* (1994), and Chrysostomou *et al.* (1997) show that the flow seems to be poorly collimated (see also the chapter by Burton & Stone). The SiO measurements by Wright *et al.* (1983, 1995, 1996) trace the outflow to within a few arcseconds of source I. In general, this flow is seen in millimetre maps with beams ≥ 3 arcsec, and therefore Wright *et al.* (1996) concluded that the flow originates primarily from the more extended gas and is not produced by narrow jets. That having been said, the associated shocked H_2 emission appears very clumpy on scales less than 1 arcsec (Stolovy *et al.* 1998; Schultz *et al.* 1999; see also the chapter by Burton and Stone).

3. Plateau de Bure interferometer observations

In the following sections, we will concentrate on results from observations we have made with the Plateau de Bure submillimetre/millimetre interferometer, the properties of which are comprehensively described by Guilloteau *et al.* (1992).

We made observations in the CH_3CN J=5–4, K=0,1,2,3,4 and $C^{34}S$ J=2–1 lines, the 86–99 GHz continuum, and the SO $J=2_2$–1_1 line (Schreyer 1997; Schreyer *et al.* in

Component	Velocity range and remarks
Hot core	$2 \leq v_{\rm lsr} \leq 7\,{\rm km\,s^{-1}}$ Position of the peak emission in different molecular lines in OMC-1, 3–4 arcsec southeast of IRc2 (Migenes *et al.* 1989) and 1–2 arcsec east of source I (Plambeck *et al.* 1995); densest and hottest cloud clump in OMC-1 with gas and dust temperatures of 150–300 K, densities of 10^7–$10^8\,{\rm cm^{-3}}$, a column density of $N(H_2) \geq 10^{24}\,{\rm cm^{-2}}$, and a mass of $\sim 10\,M_\odot$ (Genzel & Stutzki 1989); fully hydrogenated species and nitrogen-rich compounds are abundant (Blake *et al.* 1987; Sutton *et al.* 1995)
Compact ridge	$7 \leq v_{\rm lsr} \leq 9\,{\rm km\,s^{-1}}$ (Johansson *et al.* 1984) Position ~ 8 arcsec southwest of IRc2 (Plambeck & Wright 1987), centred on IRc4/5; region with quiescent gas with temperatures between 100–150 K (Genzel & Stutzki 1989); different chemistry compared to hot core: high abundance of complex oxygen-rich molecules (Blake *et al.* 1987)
Spike	$v_{\rm lsr} = 8.5\,{\rm km\,s^{-1}}$, $\Delta v = 3\,{\rm km\,s^{-1}}$ (Migenes *et al.* 1989) Defined in single-dish measurements: gas of the compact and extended ridge which arises from a small region compared to the beam (Barrett, Ho, & Myers 1977; Wilson, Downes, & Beiging 1979; Morris, Palmer, & Zuckerman 1980; Zuckerman, Morris, & Palmer 1981; Ziurys *et al.* 1981)
Extended ridge	$8 \leq v_{\rm lsr} \leq 12\,{\rm km\,s^{-1}}$ Extended gas > 40 arcsec along the position angle of 30° (Genzel & Stutzki 1989; Sutton *et al.* 1995) with embedded clumps, *e.g.*, CS1, a clump 24 arcsec northeast of IRc2 (Mundy *et al.* 1986; Wright *et al.* 1992); characterized by fairly simple carbon-rich species (Blake *et al.* 1987)
Plateau	Line centre at $7 \leq v_{\rm lsr} \leq 11\,{\rm km\,s^{-1}}$, $\Delta v = 3$–$30\,{\rm km\,s^{-1}}$, $\Delta v_{\rm full} = 100$–$200\,{\rm km\,s^{-1}}$ Consists of material in a high-velocity outflow originating from the vicinity of IRc2; shock chemistry, abundance of SO, SO_2, and CO is enhanced (Sutton *et al.* 1995; Wright *et al.* 1996)
Western clump	$8 \leq v_{\rm lsr} \leq 14\,{\rm km\,s^{-1}}$ Compact cloud clump 6 arcsec west of IRc2 with 2–3 $M_\odot$ (*e.g.*, Pauls *et al.* 1983; Masson & Mundy 1988; Migenes *et al.* 1989; Wright *et al.* 1992, 1996)

Table 2. Molecular components of the Orion-KL region

preparation). Here, we will only discuss the CH_3CN J=5–4 and $C^{34}S$ J=2–1 results, which were obtained by observations using three 15-m antennae between November 1991 and January 1992 using five different configurations for $C^{34}S$ and six for CH_3CN. In the case of the $C^{34}S$ measurements, additional observations were made with a more compact configuration of the array in February 1993. The phase reference centre of the measurements is RA = $05^h\ 32^m\ 46.9^s$, declination = $-05^\circ\ 24'\ 26.0''$ (B1950.0).

For the line observations, 128 channels of the spectral correlator were used in one band. The $C^{34}S$ J=2–1 line was centred at v_{lsr}=9 km s^{-1} in the LSB and the CH_3CN J=5–4 K=3 transition was placed at v_{lsr}=9 km s^{-1} in the USB. Since we intended to measure all fine-structure lines K=0,1,2,3,4 of the CH_3CN J=5–4 transition in a single band simultaneously, a somewhat lower velocity resolution of 1.02 km s^{-1} (312.5 kHz) was used for CH_3CN than for $C^{34}S$, where the highest velocity resolution of 0.24 km s^{-1} (78.1 kHz) was used.

In each period, the band pass and phase calibration was performed observing the quasar 3C84. An additional calibration of the phase and the amplitude was done by observing the quasar 0458-020 every 20 minutes. For the final phase calibration and data reduction, we used CLIC (Lucas 1992) and GRAPHIC (Guilloteau & Forveille 1992) in the Grenoble Software environment GAG. Zero-spacing information obtained with the IRAM 30 m telescope have been added to the $C^{34}S$ visibility data, contributing $\sim$50–90% to the total flux in the velocity range 7–11 km s^{-1}. The comparison between the CH_3CN interferometer data with IRAM 30 m data shows that, in this case, the missing flux is below the calibration errors and thus no zero-spacing information was included.

Finally, maps with 256×256 pixels with a 0.5 arcsec pixel size were produced by Fourier-transforming the calibrated visibilities, using natural weighting. The synthesized beam sizes (HPBW) are 4.7×1.8 arcsec for CH_3CN and 4.3×1.7 arcsec for $C^{34}S$ with a position angle of 16°.

3.1. Morphology in CH_3CN and $C^{34}S$

In agreement with earlier line studies (*e.g.*, Migenes *et al.* 1989; Murata *et al.* 1991; Wright *et al.* 1996; see Table 1), Figure 2 shows that the clump structure seen in CH_3CN and $C^{34}S$ is similar to that found in NH_3, $H^{13}CN$, SO, and CS. The hot core (clump $\mathcal{A}$ in Figure 2) is obviously the most intense emission region in both line transitions. The CH_3CN maps show this region to have a 'bean-like' structure, with source I located at the western periphery. The CH_3CN emission peaks at an offset of 1.5 arcsec east of source I, while the $C^{34}S$ map shows a slightly smaller offset of only 0.5 arcsec between source I and the long axis of the hot core clump. The $C^{34}S$ emission in fact peaks close to the near-infrared source n (radio source L) at v_{lsr}=6.2 km s^{-1}.

Source I was proposed by Blake *et al.* (1996) to lie behind the hot core, and to examine this hypothesis, we have analysed our high-spectral resolution $C^{34}S$ measurements. The emission at the position of source I peaks in intensity at a velocity of v_{lsr}=5.4 km s^{-1}, nearly identical to the central velocity of the SiO maser emission determined by Menten & Reid (1995), and thus this emission is probably associated with source I itself. At the position of hot core, however, the peak $C^{34}S$ emission is seen at a somewhat lower velocity of v_{lsr}=4.9 km s^{-1}, and if these different velocities are interpreted in terms of a spatial displacement, they would the support the suggestion of Blake *et al.* (1996).

Further distinct gas clumps are seen in Figure 2. Clump $\mathcal{C}$ is clearly seen in the transitions of both molecules, and is associated with the infrared source IRc6, located 6.5 arcsec northwest of IRc2. The emission at this clump peaks at $v_{lsr}(CH_3CN)$=9.5 km s^{-1}

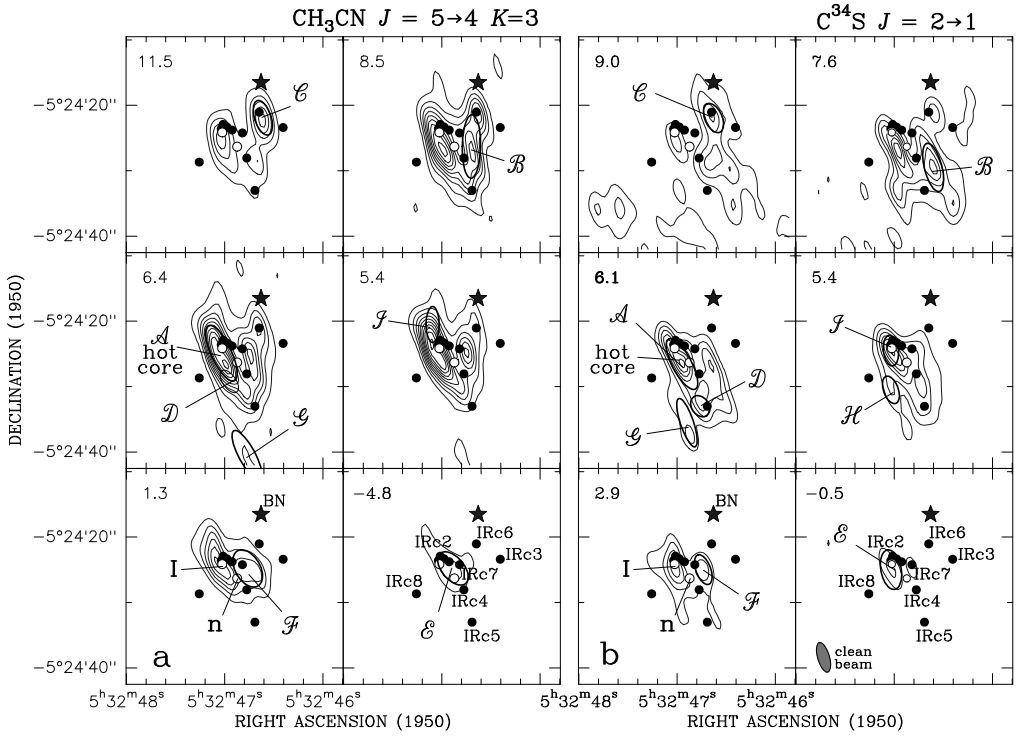

Figure 2. Six channel maps for each of CH_3CN J=5–4 (left panels) and $C^{34}S$ J=2–1 (right panels). The central velocities are given in the top left corner of each panel. Our designations for the clumps range from $\mathcal{A}$ to $\mathcal{I}$. The positions of the infrared sources IRc2–IRc8 and of the BN object (Dougados *et al.* 1993) are indicated by black dots and a star respectively. The radio source I and near-infrared source n are marked with open circles. Dashed ellipses show the half widths of the Gaussian-shaped clumps (beam-convolved).

and $v_{\rm lsr}(C^{34}S)$=9.0 km s^{-1}, quite different from that of the hot core. Clump $\mathcal{B}$ is also seen in the channel maps of both molecules, and is located at the western side of source I with an emission peak at $v_{\rm lsr} \sim 7.5\,{\rm km\,s^{-1}}$. There is quite some confusion regarding the nomenclature used for these clumps. The 'IRc6 clump' (here $\mathcal{C}$; also clump #10 of Migenes *et al.* 1989) was described as the 'western clump' by Masson & Mundy (1988), while the term 'western clump' was used by Hermsen *et al.* (1988) and Pauls *et al.* (1983; their clump A) to refer to the clump labelled as $\mathcal{B}$ here (also clump #8 of Migenes *et al.* 1989). However, it is clear that these are distinct clumps, well separated in space and velocity. In contrast to the clumps of hot core and clump $\mathcal{C}$ associated with IRc6, where the spatial location of the clumps is roughly identical in both molecules, clump $\mathcal{B}$ seems to be shifted slightly southwards in $C^{34}S$ with respect to its CH_3CN position, and it is quite possible that this gas clump belongs to the compact ridge region rather than being a true independent clump.

As discussed in Section 2, radio source I appears to play perhaps the central role in the region. With that in mind, an important result of our study is that the CH_3CN spectra show their *broadest* lines not at source I, but rather at the position of infrared source n, despite the *strongest* CH_3CN emission being found close to source I. In ad-

dition, the whole region around source n, IRc4, and IRc7 shows two clearly separated velocity components with broad line wings.

In contrast, the $C^{34}S$ spectra contain many narrow velocity components implying the existence of many small and dense cloud clumps, embedded in the more extended clump envelopes detected in CH_3CN. These small clumps have linewidths of the order of the thermal linewidth, assuming kinetic temperatures of 50–200 K. A comparison of the $C^{34}S$ spectra with those of the CH_3CN K=3 line shows an absence of redshifted $C^{34}S$ emission in the spectra around the region of IRc5, associated with the compact ridge. It thus appears that the two molecular transitions are tracing rather different gas. Determinations of the optical depths in the two lines using excitation calculations (Schreyer 1997; Schreyer *et al.*, in preparation) suggest that the optical depth for the gas observed in CH_3CN is $\gg 1$, while lower values of ≈ 0.3 are obtained for $C^{34}S$, allowing a 'deeper' look through the envelopes surrounding the clumps.

In order to derive the brightness temperature, virial mass, and volume-averaged density of each clump, we have performed a statistical analysis following the procedure given by Stutzki & Güsten (1990). This procedure decomposes a 3-dimensional intensity distribution (S_ν versus right ascension, declination, and velocity) into individual Gaussian-shaped clumps which are convolved with the clean beam. In the next step, the Gaussian profiles are deconvolved in order to obtain the 'real' values of the different quantities for the clumps. We applied this procedure for all K lines of CH_3CN J=5–4 and for $C^{34}S$ J=2–1. As a check of the reliability of the results, we varied the input parameters for this analysis. The CH_3CN dataset (including all K lines) can be fit with approximately 100 Gaussian-shaped clumps, while the $C^{34}S$ intensity distribution can be reproduced with 30–40 clumps depending on the input parameters. We stress that all clumps with amplitudes $\geq 1\sigma$ above the noise were consistently found in several fit calculations. While the central coordinates remain roughly fixed as the parameters are varied, the size and amplitude in particular are seen to be variable for the weaker intensity clumps.

The parameters of the most prominent clumps found in CH_3CN and in $C^{34}S$ are listed in Table 3, and the location and the sizes of these clumps are shown in the channel maps of Figure 2. Although the locations and sizes of these features are not exactly identical in the two lines, a uniform notation has been used for the clumps in both cases ($\mathcal{A}$,$\mathcal{B}$,$\mathcal{C}$,*etc.*). Based on the partial merging of the CH $_3$CN K=0 and K=1 lines in the spectra, the separation of clumps belonging to these lines is rather complicated, and the spatial and velocity extent of clumps found in the CH_3CN K=2 and 3 lines are similar due to their similar excitation conditions. Therefore, Table 3 shows only average quantities for these transitions[2]. In addition, Table 3 lists the virial masses $M_{\rm vir}$ and the volume-averaged densities $\langle n \rangle$ for the various clumps, which were derived for Gaussian-shaped density distributions using the FWHM of the velocity (Δv) following the expression given by Stutzki & Güsten (1990):

$$\frac{G M_{\rm vir}}{R} \sqrt{\frac{\ln 2}{2\pi}} = \frac{3\pi \Delta v^2}{8 \ln 2} \, , \qquad (1)$$

[2]We note here again that the measurements by Blake *et al.* (1996) and Wright (1996) have demonstrated that the clumpy structure depends heavily on the observed molecular line transitions. Such differences are not only produced by different excitation conditions in the gas, but can also reflect distinct chemical processes occuring in the various cloud regions.

where G is the gravitational constant and R is the half width of the geometrical mean of the beam-deconvolved major and minor axes. Due to its smallest hyperfine-splitting in the velocity range and a sufficient separation from other lines in the CH_3CN spectra, the $v_8 = 2$, $K = 2$ line was used to determine $M_{\rm vir}$.

We also carried out statistical equilibrium excitation calculations, fitting the brightness temperatures $T_{\rm b}$ of the three most prominent clumps in order to determine their kinetic temperatures $T_{\rm kin}$, densities n, and column densities $N(H_2)$. For the hot core, the derived $T_{\rm kin} > 175$ K and $n \geq 5 \times 10^6$ cm^{-3} agree well with previous studies, while $N(H_2) \sim 3 \times 10^{25}$ cm^{-2} is somewhat higher than previously estimated. For clump $\mathcal{C}$, we found a high optical depth in $C^{34}S$ with $\tau > 1$ for $T_{\rm kin} < 150$ K and $n = (5$–$1000) \times 10^6$ cm^{-3}, and therefore the estimated $C^{34}S$ column density does not trace the total H_2 column density. The lower limit of $N(H_2) = (3$–$10) \times 10^{25}$ cm^{-2} is higher than the value found for the hot core. Using the CH_3CN data (*cf.* Sutton *et al.* 1986), we find a temperature of $T_{\rm kin} > 110$ K, at least for the gas in the outer envelope of clump $\mathcal{C}$. Finally, for clump $\mathcal{B}$ (which shows no counterpart in continuum emission), we found lower temperatures ($T_{\rm kin} \geq 95$ K), densities ($n \geq 10^6$ cm^{-3}), and column densities ($N(H_2) \approx 9 \times 10^{24}$ cm^{-2}) than the hot core.

3.2. Rotation around source I

To examine the velocity structure in the hot core/compact ridge region, we took a cut along the long axis of clump $\mathcal{A}$ (hot core) to make position-velocity diagrams for both CH_3CN and $C^{34}S$. In particular, we wanted to see if the region the region breaks up into single clumps showing a chaotic motion as discussed by Migenes *et al.* (1989) and Plambeck *et al.* (1995), or if there is any evidence for systematic gas motion around hot core. The cut was made at a position angle of 15° at a distance of 0.3 arcsec from source I (see Figure 3b and d): the resulting position-velocity diagrams are shown in Figure 3a and c, where the intensity is plotted against the distance from source I.

The position-velocity maps for both molecules show a systematic velocity field within a radius of 3–4 arcsec around source I. Since they have four times better velocity resolution and a smaller optical depth, the $C^{34}S$ measurements show more details than the CH_3CN measurements, but both maps show a clear suggestion of rotation of the gas around source I. This result is supported by the fact that the much smaller SiO maser ring proposed in the models of Barvainis (1984) and Plambeck *et al.* (1990) rotates in the same direction (although see Section 2.1. for an alternative model, in which the SiO masers arise in a bipolar outflow from Source I: Greenhill *et al.* 1998; Doeleman *et al.* 1999).

We compared the velocity field shown in Figures 3a and c with a simple model of Keplerian motion with the mass distribution introduced by Vogel *et al.* (1985). In the rotational equilibrium model, a central star and a cloud mass increasing linearly with radius are assumed. Following earlier models discussed by Vogel *et al.* (1985), Habing & Macdonald (1991), Murata *et al.* (1991), and Wilner, Wright, & Plambeck (1994), we used a central mass of 25 $M_\odot$ in agreement with the mass of a main-sequence star with luminosity 10^5 $L_\odot$ (Garmany, Conti, & Chiosi 1982) and a cloud radius of 10 arcsec adopted from the line measurements. For the gas mass, we took values between the limits found by the virial and dust mass estimates for clump $\mathcal{A}$ (the hot core). The outer cloud radius was assumed to be 10 arcsec. Changing the cloud mass within the limits and varying the extent of the outer cloud (by 25%) had only a weak influence on the resulting rotation curve compared to that induced by varying the inclination angle.

Clump	x_0 5^h32^m	y_0 $-5°24'$	v_{lsr} [km s^{-1}]	$\Delta v_{1/2}$ [km s^{-1}]	$\Delta x_1 \times \Delta x_2$ [″×″]	ϕ [°]	FWHM [″]	dv/dl [km s^{-1}]	ϕ_v [°]	M_{vir} [$M_\odot$]	$\langle n \rangle \times 10^8$ [cm^{-3}]
(1)	(2)	(3)	(4)	(5)	(6)	(7)	(8)	(9)	(10)	(11)	(12)
					CH_3CN (averaged over all K lines)						
$\mathcal{A}$	47.033^s	24.90″	5.8	6.3	8.1×2.4	27.8	4.17	0.256	152	70	2.9
$\mathcal{B}$	46.700^s	26.30″	8.1	5.2	8.6×1.6	174.8	3.45	0.482	91	40	2.8
$\mathcal{C}$	46.613^s	21.90″	11.7	6.4	2.9×1.7	25.1	3.17	1.110	−117	38	11.0
$\mathcal{D}$	46.953^s	29.20″	8.4	2.3	(4.0×2.0)	(86.9)	2.20	0.340	−46	≤5	≤1.0
$\mathcal{E}$	46.887^s	24.80″	−5.0	5.3	4.5×1.4	64.9	4.37	0.354	−105	29	6.3
$\mathcal{F}$	46.767^s	24.80″	1.8	3.8	4.4×2.8	55.1	3.96	0.550	47	21	1.7
$\mathcal{G}$	46.773^s	40.50″	5.3	3.3	7.2×1.4	32.5	3.30	0.378	−130	15	1.5
$\mathcal{I}$	47.093^s	20.50″	5.4	4.0	(5.5×2.0)	(157.9)	2.00	0.805	98	≤13	≤5.7
					$C^{34}S$						
$\mathcal{A}$	46.958^s	26.50″	6.1	4.1	7.5×2.1	31.2	3.82	0.339	26	28	1.5
$\mathcal{B}$	46.614^s	29.45″	7.6	3.3	6.3×2.2	11.1	3.71	0.362	60	17	1.1
$\mathcal{C}$	46.627^s	21.83″	9.0	2.5	2.5×1.4	66.9	3.27	0.129	−94	4.8	2.5
$\mathcal{D}$	46.764^s	33.00″	6.1	1.7	(2.4×3.5)	(110.5)	2.83	0.324	−108	≤3.4	≤0.5
$\mathcal{E}$	47.030^s	24.97″	−0.5	2.2	4.6×2.4	5.9	3.81	0.369	2	6.6	0.6
$\mathcal{F}$	46.736^s	24.94″	2.9	3.5	2.3×1.7	36.6	3.06	0.188	−74	10	4.4
$\mathcal{G}$	46.900^s	35.53″	8.0	1.6	6.5×1.1	20.1	2.78	0.186	−16	2.8	0.5
$\mathcal{H}$	47.035^s	30.52″	5.4	1.3	2.9×1.0	36.0	2.75	0.323	−134	1.2	0.8
$\mathcal{I}$	47.034^s	24.50″	8.0	0.8	2.6×1.1	156.8	3.05	0.037	−120	0.4	0.3

Table 3. Parameters of the most prominent clumps observed in CH_3CN and $C^{34}S$ in Orion-KL. (1) clump name; (2) RA (B1950); (3) declination (B1950); (4) lsr-velocity corresponding to K=3; (5) clump velocity FWHM; (6) beam-deconvolved FWHM of the two principal spatial axes (convolved values are shown in parentheses if the clump is too small for deconvolution); (7) beam-deconvolved orientation angle (counter-clockwise from north; convolved values in parentheses); (8) geometrical mean of the beam-deconvolved major and minor axes; (9) clump internal velocity gradient; (10) direction of the internal velocity gradient (counter-clockwise from west); (11) virial mass; (12) volume-averaged density. Radio source I is at 47.085^s, 23.936″, and the two radio components associated with infrared source n are at 46.929^s, 25.927″ and 46.924^s, 26.292″ (Menten & Reid 1995).

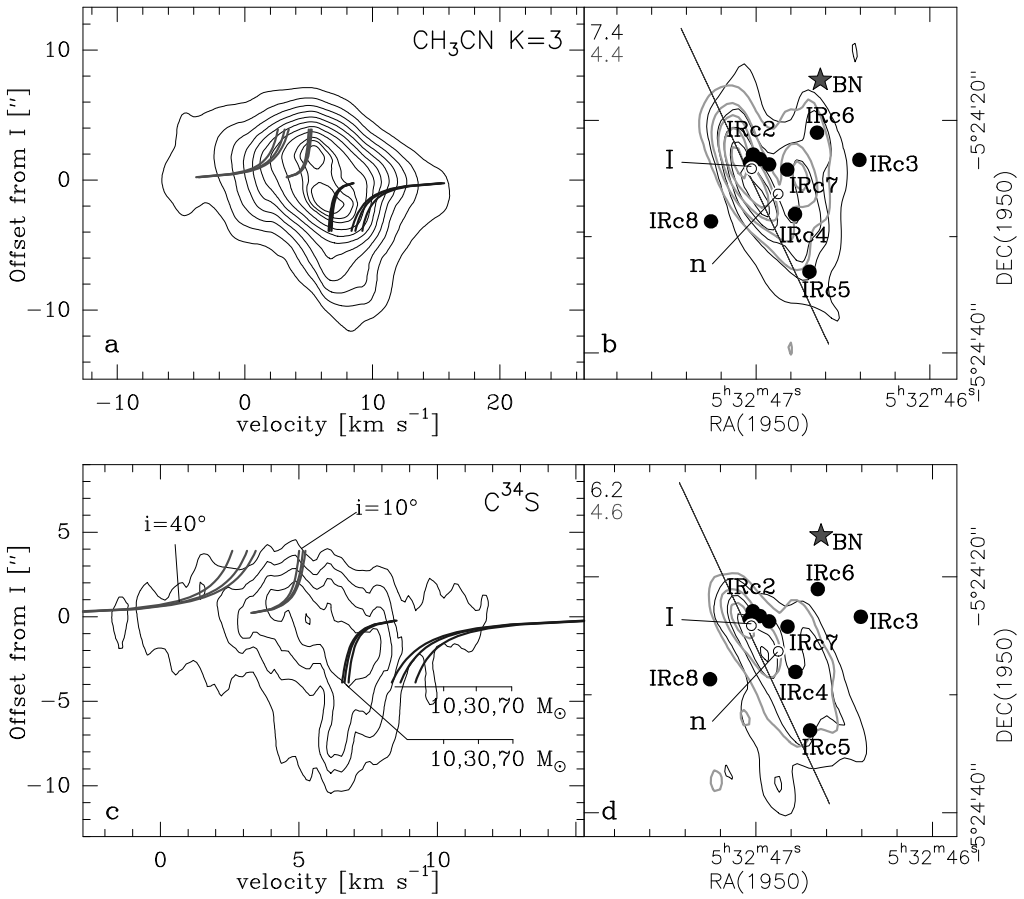

Figure 3. **a.** Position-velocity map through the long axis of clump $\mathcal{A}$ (PA=15°) in CH_3CN K=3. Contours are at 0.5–4.5 K km s^{-1} in 0.5 K km s^{-1} steps, and then 4.7, 4.9, and 5.1 K km s^{-1}. The gas within ±3 arcsec of source I shows a systematic velocity field modeled with Keplerian rotation curves $v = f$(thick lines) for cloud masses 10, 30, and 70 $M_\odot$ and inclination angles $i = 10°$ and 40° around a central star of 25 $M_\odot$. **b.** CH_3CN channel maps at v_{lsr}=7.4 km s^{-1} (black) and v_{lsr}=4.4 km s^{-1} (grey). Contours are at 0.5–6 Jy beam^{-1} in 1.0 Jy beam^{-1} steps. The line indicates the cut of the position-velocity map. **c.** Position-velocity map for $C^{34}S$. Contours are at 0.5–2.5 K km s^{-1} in 0.5 K km s^{-1} steps. The rotation curves are the same as in **a.** **d.** $C^{34}S$ channel maps at v_{lsr}=6.2 km s^{-1} (black) and at v_{lsr}=4.6 km s^{-1} (grey). Contours are at 0.35–4 Jy beam^{-1} in 0.7 Jy beam^{-1} steps.

The curves calculated for cloud masses of 10, 30, and 70 $M_\odot$ and inclination angles of $i = 10°$ and 40° are plotted in Figures 3a and c as thick lines. The curves were centred at $v_{lsr} = 59$ km s^{-1}. Although an inclination angle on the order of 45° fits better in the much smaller maser ring models of Barvainis (1984) and Plambeck *et al.* (1990), we find that an inclination between 5–15° fits the gas motion better in Figure 3, especially in the $C^{34}S$ data.

Within a radius of $r \pm 4$ arcsec, the rotation curves roughly coincide with the velocity field of the gas near source I. The velocity difference between the 'northern' and the 'southern' gas at 1.5–2 km s^{-1} is best fit using an inclination angle of $\sim 10^{\circ}$, while for $r > 4$ arcsec, no acceptable model fit is found. This suggests that the more distant gas is not participating in the rotation. We should note the results are influenced by the fact that the region of the compact ridge included in the analysis shows a somewhat different lsr-velocity, mainly in the range $v_{\rm lsr} \approx 7$–8 km s^{-1}, than the hot core, which has $v_{\rm lsr} \approx 4$–6 km s^{-1}.

At the position of source I, the line emission shows the largest velocity dispersion, with $\Delta v = 13$ km s^{-1} for $C^{34}S$ and $\Delta v = 22$ km s^{-1} for CH_3CN, thus implying the highest rotation velocity near this central object. The velocity dispersion decreases with increasing distance from source I. This fact favours the possibility of a rotating gas motion inside a radius of 1350–1800 AU (= 3–4 arcsec) around source I, on the order of twice the extent of the dust disks seen around low-mass stars in the Orion Trapezium Cluster with the Hubble Space Telescope (McCaughrean & O'Dell 1996; see also the chapter by McCaughrean).

Previous studies of the gas motion around the hot core were performed on larger scales than here (see, *e.g.*, Vogel *et al.* 1985; Habing & Macdonald 1991; Murata *et al.* 1991; Wilner *et al.* 1994), and these indicated a rotation of the northern gas condensation (known as CS1) and the compact ridge around a common centre, a finding supported by the clear difference in their central lsr-velocities. Most of these studies also made a Keplerian fit in their position-velocity diagrams, but the resulting rotation direction is in the opposite sense to that which we see in Figure 3, and to that which is derived from the SiO maser observations and included in the SiO ring models by Barvainis (1984) and Plambeck *et al.* (1990).

In contrast to the hypothesis that there is rotating gas in the hot core region, Plambeck *et al.* (1995) concluded from the clumpy structure of the hot core/compact ridge region (see, *e.g.*, the high-resolution data of Migenes *et al.* 1989) that there is no evidence for such organized gas motion. There are two ways of reconciling their conclusion with the data shown in Figure 3: first, the gas of the more extended envelope or single gas clumps may be coupled to the rotating gas disk around source I; second, the spatial resolution of our data may be too low to clearly separate rotating gas associated with source I and gas related to the hot core cloud clump.

Finally, high spatial resolution SiO measurements by Chandler & DePree (1995), Wright *et al.* (1995), and Blake *et al.* (1996) show a compact flattened gas/continuum structure around source I at a position angle of $\sim$50–60° and with a clear offset from the centre of the hot core. To date, no other line study has shown position-velocity cuts comparable to ours, and evidence for a systematic gas motion has come from a shift of the emission peak in the SiO channel maps by Chandler & DePree (1995). Only future measurements at higher spatial resolution will be able to distinguish definitely between gas motion in the hot core and around source I, but in the meantime, the evidence does appear to point towards rotation of gas around source I.

3.3. The western clump: a new site of star formation?

In order to provide new insight into the known outflow systems in Orion-KL, we examined the distribution of the red- and blue-shifted emission in the broad line wings of CH_3CN, which traces low-velocity gas. Because the various K lines are partially merged, we selected the $K = 3$ line as showing the best separated line wings, and we re-

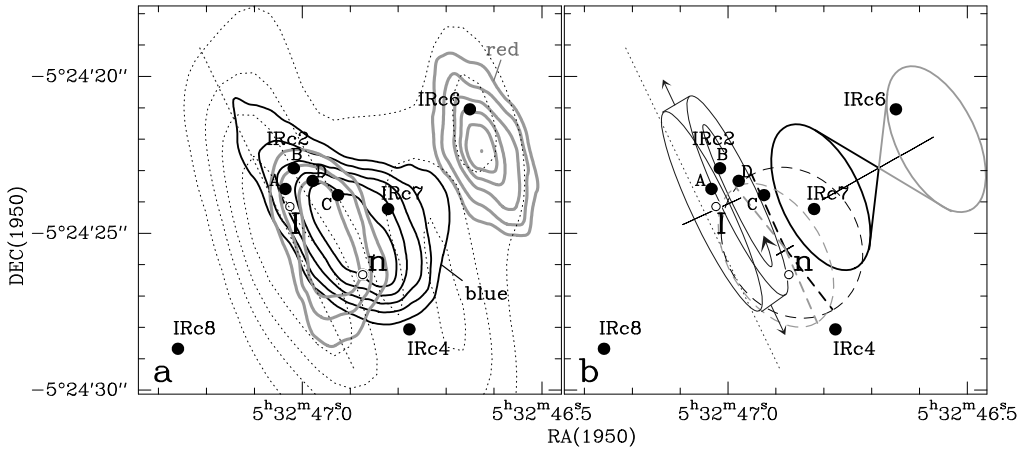

Figure 4. **a.** Overlay of the integrated intensities of the line wings of the CH_3CN $K=3$ line in the velocity ranges $-63 \leq v_{lsr} \leq -23\,\mathrm{km\,s^{-1}}$ (black lines) and $15 \leq v_{lsr} \leq 20\,\mathrm{km\,s^{-1}}$ (thick grey thick lines). The dotted contour are the channel map of CH_3CN $K=3$ at v_{lsr}=7.4 $\mathrm{km\,s^{-1}}$ and the dashed straight line shows the cut of the position-velocity map in Figure 3. **b.** Possible interpretation of the red- and blue-shifted line emission in the region around IRc2 with (1) an expanding and rotating gas disk/torus around source I; (2) a bipolar outflow centred between IRc6 and IRc7; and (3) another bipolar flow orientated along the line-of-sight and located near source n.

duced its blue-shifted wing emission in order to exclude velocity ranges covering contributions from the $K=2$ red-shifted wing emission.

Figure 4a shows the integrated red- and blue-shifted line wing emission maps superimposed. Although any interpretation of the emission distribution is not without ambiguities, we have also examined the CH_3CN spectra in detail (Schreyer 1997; Schreyer *et al.*, in preparation), and propose that there are three outflow systems at work:

(i) There appears to be a poorly-collimated outflow (with two broad bipolar lobes) originating from a position between IRc6 and IRc7, with a central velocity of $v_{lsr} \approx 9\,\mathrm{km\,s^{-1}}$, and covering a velocity range of $\Delta v \approx 30\,\mathrm{km\,s^{-1}}$. In this picture, the infrared sources IRc6 and IRc7 would be explained as scattered light escaping through the bipolar outflow lobes. This flow is not the same as the known high-velocity flow described in Section 2.3., which spans a much larger velocity range and whose red- and blue-shifted emission regions are swapped with respect to the flow seen here.

(ii) The red- and blue-shifted line emission roughly centred on source I traces the expanding gas shell/torus described in Section 2.3.. It is interesting to note that these emission regions lie mainly to the western side of the 'cut line' through centre of hot core, as does source I itself.

(iii) There appears to be another bipolar outflow which originates near source n and is centred at a velocity $v_{lsr} \approx 23\,\mathrm{km\,s^{-1}}$. The axis of the flow seems to be closer to the line-of-sight than that of the outflow centred on IRc6/IRc7 described above.

Figure 4b shows a model of the three flow systems. In order to resolve and to clarify the various gas flows, further line measurements with sub-arcsecond spatial resolution are necessary. We should note that apart from the broad CH_3CN lines in the regions of IRc6/IRc7, source I, and source n, much smaller line wings are also present in the region, *e.g.*, to the east of the hot core. We did not consider these data for the wing mapping presented here because of the complicated line profile structure, but we cannot exclude the possibility that other flow systems might be present, which may be found in both higher spatial and spectral resolution observations.

Can we now identify a stellar or protostellar driving source for the new outflow apparently originating from somewhere between the infrared sources IRc6 and IRc7? VLA radio contiuum measurements (*e.g.*, Garay *et al.* 1987; Felli *et al.* 1993; Menten & Reid 1995; see also the chapter by Felli & Churchwell) did not reveal any compact radio continuum source at this position, and millimetre continuum measurements with beam sizes $\geq$ 15 arcsec found only extended dust emission from near IRc6 (*e.g.*, Wright *et al.* 1995; Blake *et al.* 1996). However, we note that in Section 3.1., we discussed the dense clump $\mathcal{C}$ (see Table 3) near IRc6, which has a mass of 2–3 $M_\odot$, a large H_2 column density, and a high temperature of $\geq$ 110 K. These appear to be strong hints for ongoing low-mass star formation in this region.

4. Conclusions and Outlook

The main results of our Plateau de Bure observations can be summarized as follows:

- The $C^{34}S$ spectra led to the detection of a large number of small and dense clumps with linewidths of the order of the thermal linewidth, while the CH_3CN measurements trace only the more extended cloud envelopes of the densest cloud cores.
- Looking at the broad line wings of the CH_3CN spectra, we conclude that the inner cavity surrounded by the denser clumps $\mathcal{A}$, $\mathcal{B}$, $\mathcal{C}$, and $\mathcal{D}$ is filled by lower-density gas in a very turbulent state.
- Although the $C^{34}S$ spectra imply the existence of many small and dense cloud clumps, position-velocity cuts along the long axis of the hot core (clump $\mathcal{A}$) in CH_3CN and $C^{34}S$ show evidence for a systematic velocity fields whose pattern suggests rotation of the gas around source I.
- We found no emission related to the Orion-KL high-velocity outflow in either the CH_3CN or $C^{34}S$ measurements, but maps in the broad CH_3CN line wings indicates at least two different low-velocity gas flows in the Orion-KL region, namely the rotating and expanding gas shell around source I and a poorly collimated bipolar outflow centred near the infrared source n.
- We have identified a new found bipolar outflow centred between IRc6 and IRc7, and the presence there of a small, warm, and dense cloud clump provide strong indications of on-going low-mass star formation in this region.

By integrating the various high-resolution infrared and millimetre data, we are approaching an unified model for the Orion-KL region, and such data are extremely important if we want to obtain a more detailed picture of high-mass star formation in this region. There is much evidence that source I is the main source of the large luminosity

emitted by the region, and we have presented evidence for gas rotating around source I. The presence of very young low-mass stars associated with the young high-mass stars has often been debated, but remains to be confirmed through observations. Higher angular resolution measurements of the mid- and far-infrared emission, as well as observations in higher molecular line transitions with very good spatial and spectral resolution are necessary in order to clarify the nature of the deeply embedded stellar source(s) and their relation to the ongoing outflow activities. In addition, the underlying reasons for chemical differentiation in the region need to be investigated. Another open question concerns the origin of the turbulent gas in the inner cavity of the Orion-KL region: possible sources of the turbulent motion include source I, source n, the impact of blue-shifted low-velocity outflow material driven by a source located close to IRc6, and a mixture of two or more of these. As the capabilities of existing interferometers are extended and as new instruments such as the VLTI, the SMA, and ALMA come into operation, we can anticipate significant further progress in our understanding of the Orion-KL region.

Acknowledgments. We are grateful to the organizers of the meeting for the opportunity to review the fascinating millimetre/submillimetre data on the Orion-KL region. We thank Rolf Güsten (MPI für Radioastronomie, Bonn) for initiating the PdB project and for a critical discussion of the paper. In addition, we thank Geoffrey Blake for permission to use his molecular line images in this paper. KS is supported by the "BMBF-Verbundforschungsprojekt Astronomie/Astrophysik" No. 053JN13A1.

References

Allen, D. A., & Burton, M. G. 1993, Nature, 363, 54

Barrett, A. H., Ho, P. T. P., & Myers, P. C. 1977, ApJ, 211, L39

Barvainis, R. 1984, ApJ, 279, 358

Baud, B., Bieging, J. H., Plambeck, R. L., Thornton, D. D., Welch, W. J., & Wright, M. C. H. 1980, in *Interstellar Molecules*, ed. B. H. Andrew, IAU Symposium 87, (Reidel: Dordrecht), p545

Becklin, E. E., & Neugebauer, G. 1967, ApJ, 147, 799

Beckwith, S., Persson, S. E., Neugebauer, G., & Becklin, E. E. 1978, ApJ, 223, 464

Blake, G. A., Mundy, L. G., Carlstrom, J. E., Padin, S., Scott, S. L., Scoville, N. Z., & Woody, D. P. 1996, ApJ, 472, L49

Blake, G. A., Sutton, E. C., Masson, C. R., & Phillips, T. G. 1987, ApJ, 315, 621

Chandler, C. J., & DePree, C. G. 1995, ApJ, 455, L67

Chelli, A., Perrier, C., & Léna, P. 1984, ApJ, 280, 163

Chernin, L. M., & Wright, M. C. H. 1996, ApJ, 467, 676

Chrysostomou, A., Burton, M. G., Axon, D. J., Brand, P. W. J. L., Hough, J. H., Bland-Hawthorn, J., & Geballe, T. R. 1997, MNRAS, 289, 605

Churchwell, E., Wood, D. O. S., Felli, M., & Massi, M. 1987, ApJ, 321, 516

Doeleman, S. S., Lonsdale, C. J., & Pelkey, S. 1999, ApJ, 510, L55

Dougados, C., Léna, P., Ridgway, S. T., Christou, J. C., & Probst, R. G. 1993, ApJ, 406, 112

Downes, D., Genzel, R., Becklin, E. E., & Wynn-Williams, C. G. 1981, ApJ, 244, 869

Drapatz, S., Haser, L., Hofmann, R., Oda, N., & Iyengar, K. V. K. 1983, A&A, 128, 207

Erickson, N. R., Goldsmith, P. F., Snell, R. L., Berson, R. L., Huguenin, G. R., Ulich, B. L., & Lada, C. J. 1982, ApJ, 261, L103

Felli, M., Churchwell, E., Wilson, T. L., & Taylor, G. B. 1993, A&AS, 98, 137

Foy, R., Chelli, A., Léna, P., & Sibille, F. 1979, aap, 79, L5

Garay, G., Moran, J. M., & Reid, M. J. 1987, ApJ, 314, 535

Garmany, C. D., Conti, P. S., & Chiosi, C. 1982, ApJ, 263, 777

Gaume, R. A., Wilson, T. L., Vrba, F. J., & Johnstone, K. J., & Schmid-Burgk, J. 1998, ApJ, 493, 940

Genzel, R., Downes, D., Ho, P. T. P., & Bieging, J. 1982, ApJ, 259, L103

Genzel, R., Reid, M. J., Moran, J. M., & Downes, D. 1981, ApJ, 244, 884

Genzel, R., & Stutzki, J. 1989, ARA&A, 27, 41

Gezari, D. Y. 1992, ApJ, 396, L43

Gezari, D. Y., Backman, D. E., & Werner, M. W. 1998, ApJ, 509, 283

Grasdalen, G. L., Gehrz, R. D., & Hackwell, J.A. 1981, in *Infared Astronomy*, eds. C. G. Wynn-Williams & D. P. Cruikshank, (Dordrecht: Reidel), p179

Greenhill, L. J., Gwinn, C. R., Schwartz, C., Moran, J. M., & Diamond, P. J. 1998, Nature, 396, 650

Guilloteau, S., Delannoy, J., Downes, D., Greve, A., Guélin, M., Lucas, R., Morris, D., Radford, S. J. E., Wink, J., Cernicharo, J., Forveille, T., Garcia-Burillo, S., Neri, R., Blondel, J., Perrigourad, A., Plathner, D., & Torres, M. 1992, A&A, 262, 624

Guilloteau, S., & Forveille, T. 1992, *Grenoble Image and Line Data Analysis System* (GILDAS), Version 2.0

Habing, R. J., & Macdonald, G. H. 1991, A&A, 252, 705

Henning, T. 1990, Fund. Cosmic Physics, 14, 322

Hermsen, W., Wilson, T. L., & Bieging, J. H. 1988, A&A, 201, 276

Jaffe, D. T., Davidson, J. A., Dragovan, M., & Hildebrand, R. H. 1984, ApJ, 284, 637

Johansson, L. E. B., Andersson, C., Ellder, J., Friberg, P., Hjalmarson, A., Hoglund, B., Irvine, W. M., Olofsson, H., & Rydbeck, G. 1984, A&A, 130, 227

Kleinmann, D. E., & Low, F. J. 1967, ApJ, 149, L1

Lee, T. J., Beattie, D. H., Pickup, D. A., & Geballe, T. R. 1983, A&A, 127, 417

Lonsdale, C. J., Becklin, E. E., Lee, T. J., & Stewart, J. M. 1982, AJ, 87, 1819

Lucas, R. 1992, *Continuum and Line Interferometer Calibration* (CLIC), Version 2.2

Mangum, J. G., Wootten, A., & Plambeck, R. L. 1993, ApJ, 409, 282

Masson, C. R., Claussen, M. J., Lo, K. Y., Moffet, A. T., Phillips, T. G., Sargent, A. I., Scott., S. L., & Scoville, N. Z. 1985, ApJ, 295, L47

Masson, C. R., Lo, K. Y., Phillips, T. G., Sargent, A. I., Scoville, N. Z., & Woody, D. P. 1987, ApJ, 319, 446

Masson, C. R., & Mundy, L. G. 1988, ApJ, 324, 538

McCaughrean, M. J., & O'Dell, C. R. 1996, AJ, 111, 1977

Menten, K. M., & Reid, M. J. 1995, ApJ, 445, L157

Migenes, V., Johnston, K. J., Pauls, T. A., & Wilson, T. L. 1989, ApJ, 347, 294

Minchin, N. R., Hough, J. H., McCall, A., Burton, M. G., McCaughrean, M. J., Aspin, C., Bailey, J. A., Axon, D. J., & Sato, S. 1991, MNRAS, 248, 715

Minh, Y. C., Ohishi, M., Roh, D. G., Ishiguro, M., & Irvine, W. M. 1993, ApJ, 411, 773

Morris, M., Palmer, P., & Zuckerman, B. 1980, ApJ, 237, 1

Mundy, L. G., Scoville, N. Z., Bååth, L. B., Masson, C. R., & Woody, D. P. 1986, ApJ, 304, L51

Murata, Y., & Hasegawa, T. 1990, ApJ, 359, 125

Murata, Y., Kawabe, R., Ishiguro, M., Hasegawa, T., & Hayashi, M. 1991, in *Fragmentation o f Molecular Cloud and Star Formation*, IAU Symposium 147, eds. E. Falgarone, F. Boulanger, & G. Duvert, (Dordrecht: Kluwer), p357

Pauls, T. A., Wilson, T. L., Bieging, J. H., & Martin, R. N. 1983, A&A, 124, 23

Plambeck, R. L., & Wright, M. C. H. 1987, ApJ, 317, L101

Plambeck, R. L., Wright, M. C. H., & Carlstrom, J. E. 1990, ApJ, 348, L65

Plambeck, R. L., Wright, M. C. H., Mundy, L. G., & Looney, L. W. 1995, ApJ, 455, L189

Plambeck, R. L., Wright, M. C. H., Welch, W. J., Bieging, J. H., Baud, B., Ho, P. T. P., & Vogel, S. N. 1982, ApJ, 259, 617

Rao, R., Crutcher, R. M., Plambeck, R. L., & Wright, M. C. H. 1998, ApJ, 502, L75

Rieke, G. H., Low, F. J., & Kleinmann, D. E. 1973, ApJ, 186, L7

Schilke, P., Walmsley, C. M., Pineau des Forêts, G., Roueff, E., Flower, D. R., Guilloteau, S. 1992, A&A, 256, 595

Schulz, A., Henkel, C., Beckmann, U., Kasemann, C., Schneider, G., Nyman, L. Å., Persson, G., Gunnarsson, L. G., & Delgado, G. 1995, A&A, 295, 183

Schultz, A. S. B., Colgan, S. W. J., Erickson, E. F., Kaufman, M. J., Hollenbach, D. J., O'Dell, C. R., Young, E. T., & Chen, H. 1999, ApJ, 511, 282

Schreyer K. 1997, PhD thesis, Friedrich-Schiller-Universität Jena

Scoville, N. Z., Hall, D. N. B., Kleinmann, S. G., & Ridgway, S. T. 1982, ApJ, 253, 136

Scoville, N. Z., Kleinmann, S. G., Hall, D. N. B., & Ridgway, S. T. 1983, ApJ, 275, 201

Stolovy, S. R., Burton, M. G., Erickson, E. F., Kaufman, M. J., Chrysostomou, A., Young, E. T., Colgan, S. W. J., Axon, D. J., Thompson, R. I., Rieke, M. J., & Schneider, G. 1998, ApJ, 492, L151

Stutzki, J., & Güsten, R. 1990, ApJ, 356, 513

Sugai, H., Usuda, T., Kataza, H., Tanaka, M., Inoue, M. Y., Kawabata, H., Takami, H., Aoki, T., & Hiromoto, N. 1994, ApJ, 420, 746

Sutton, E. C., Blake, G. A., Genzel, R., Masson, C. R., & Phillips, T. G. 1986, ApJ, 311, 921

Sutton, E. C., Peng, R., Danchi, W. C., Jaminet, P. A., Sandell, G., Russell, A. P. G. 1995, ApJS, 97, 455

Thronson, H. A., Harper, D. A., Bally, J., Dragovan, M., Mozurkewich, D., Greenhouse, M. A., Schwartz, P. R., Smith, H. A., Bieging, J. A., Loewenstein, R. F., & Lada, C. J. 1986, AJ, 91, 1350

Vogel, S. N., Wright, M. C. H., Plambeck, R. L., & Welch, W. J. 1984, ApJ, 283, 655

Werner, M. W., Capps, R. W., & Dinerstein, H. L. 1983, ApJ, 265, L13

Werner, M. W., Gatley, I., Becklin, E. E., Harper, D. A., Loewenstein, R. F., Telsco, C. M., & Thronson, H. A. 1976, ApJ, 204, 420

Wilner, D. J., Wright, M. C. H., & Plambeck, R. L. 1994, ApJ, 422, 642

Wilson, T. L., Downes, D., & Bieging, J. 1979, A&A, 71, 275

Wilson, T. L., Gaume, R. A., Johnston, K. J., Schmid-Burgk, J., 1996, in *Science with Large Millimetre Arrays*, proc. ESO-IRAM-NFRA-Onsala Workshop, ed. P. A. Shaver, (Berlin: Springer-Verlag), p177

Wright, M. C. H., Carlstrom, J. E., Plambeck, R. L., & Welch, W. J. 1990, AJ, 99, 1299

Wright, M. C. H., & Plambeck, R. L. 1983, ApJ, 267, L115

Wright, M. C. H., Plambeck, R. L., Mundy, L. G., & Looney, L. W. 1995, ApJ, 455, L185

Wright, M. C. H., Plambeck, R. L., Vogel, S. N., Ho, P. T. P., & Welch, W.J. 1983, ApJ, 267, L41

Wright, M. C. H., Plambeck, R. L., & Wilner, D. J. 1996, ApJ, 469, 216

Wright, M. C. H., Sandell, G., Wilner, D. J., & Plambeck, R. L. 1992, ApJ, 393, 225

Wright, M. C. H., & Vogel, S. N. 1985, ApJ, 297, L11

Wynn-Williams, C. G., Genzel, R., Becklin, E. E., & Downes, D. 1984, ApJ, 281, 172

Ziurys, L., Martin, R., Pauls, T., & Wilson, T. L. 1981, A&A, 104, 288

Zuckerman, B., Morris, M., & Palmer, P. 1981, ApJ, 250, L39